Reduction of the GPM IMERG Final Run Underestimation in the Eastern Himalaya

XUELONG CHEN,[a] XIN XU,[a] QIANG ZHANG,[a] YAJING LIU,[a] DELIANG CHEN,[b] AND YAOMING MA[a]

[a] *Land-Atmosphere Interaction and Its Climatic Effects Group, State Key Laboratory of Tibetan Plateau Earth System, Environment and Resources), Institute of Tibetan Plateau Research, Chinese Academy of Sciences, Beijing, China*
[b] *Department of Earth System Science, Tsinghua University, Beijing, China*

(Manuscript received 9 July 2024, in final form 18 February 2025, accepted 23 February 2025)

ABSTRACT: The Yarlung Zsangbo Grand Canyon (YGC) in the eastern Himalaya is one of the deepest canyons in the world. Satellite precipitation products should be assessed and calibrated before their applications in this remote mountain area. A new rain gauge network was installed in the YGC in November 2018, since then the network observation data were utilized to calibrate the Integrated Multi-satellitE Retrievals for Global Precipitation Measurement V06 Final Run (IMERG-F) product. The evaluation demonstrated that the IMERG-F data reasonably captured the observed seasonal and diurnal variations in the precipitation but with much weaker seasonal and diurnal variations compared with the gauge data. The IMERG-F overestimated/underestimated the hourly light/heavy precipitation frequency, leading to a significant underestimation of daily and monthly rainfall amounts. The rainfall produced by the two layers of cloud in the mountainous region cannot be captured by the IMERG-F algorithm, which causes the underestimation of total rainfall. To address this issue, we applied a cumulative distribution function (CDF) calibration, which successfully reduced the mean bias of hourly and monthly rainfall for IMERG-F from -0.11 mm h^{-1} and -95.0 mm month^{-1} to 0.03 mm h^{-1} and -5.2 mm month^{-1}. The mean biases of the daily light, moderate, and heavy rainfall decreased from -0.93, -1.02, and 4.71 to 0.13, -0.13, and 3.24 mm day^{-1}, respectively. The CDF method can effectively correct the underestimation bias in IMERG-F. This study has implications for the application of satellite rainfall products to global mountain areas.

SIGNIFICANCE STATEMENT: The Yarlung Zsangbo Grand Canyon (YGC) is one of the deepest canyons in the world. Precipitation in the YGC often brings natural disasters to local communities, which affect their livelihood. Remotely sensed precipitation products can be valuable for this region if they are adequately calibrated and assessed using rain gauges. A new rain gauge network was installed in the YGC in November 2018, and more than 3 years of observations were utilized to evaluate the Integrated Multi-satellitE Retrievals for Global Precipitation Measurement (GPM) (IMERG) precipitation product. The evaluation results demonstrated that the IMERG significantly underestimated rainfall at the daily and monthly time scales. Some possible mechanisms for this underestimation were investigated to help scientists improve the satellite precipitation products for this region.

KEYWORDS: Convective clouds; Gauges; Satellite observations; Downscaling; Mountain meteorology

1. Introduction

Global reanalysis data may not be suitable for studying the precipitation in the mountainous areas of the Yarlung Zsangbo Grand Canyon (YGC) (Chen et al. 2023), located in the southeastern Tibetan Plateau. In the remote mountainous regions of the eastern Himalayas, the sparse distribution of rain gauges limits the representativeness of ground-based measurements. This poses a significant challenge for accurate precipitation estimation in this area.

Satellite-based precipitation products offer the unique advantage of observing precipitation over areas where ground instruments are sparse or absent, offering a potential alternative to ground-based precipitation estimates in the YGC. In this poorly gauged region, the use of remotely sensed precipitation products with high spatial–temporal resolution should be explored. However, how accurate and reliable satellite precipitation products are for the YGC region is still unclear.

The Global Precipitation Measurement (GPM) mission, which provides high temporal resolution data, has the potential to capture the seasonal and diurnal variations of precipitation in the YGC. Previous studies have evaluated the GPM's performance on the Tibetan Plateau at daily, monthly, and annual scales. However, to our knowledge, no study has assessed GPM data at subdaily time scales specifically for the YGC. Evaluating the capability of GPM satellite precipitation products in this region requires comparison with data from a well-established network of ground-based precipitation stations. Rain gauge observation data have never been collected before we started the investigation of the precipitation process in the water vapor channel of the Yarlung Zsangbo Grand Canyon (INVC) project in the southeastern Tibetan Plateau (TP) (Chen et al. 2024a).

The Tropical Rainfall Measuring Mission (TRMM), a collaborative project between American National Aeronautics and Space Administration (NASA) and the Japan Aerospace Exploration Agency (JAXA), launched in 1997, provided the first space-based radar capable of measuring rainfall over both land and ocean. It helped scientists to improve weather

Corresponding author: Xuelong Chen, x.chen@itpcas.ac.cn

DOI: 10.1175/JHM-D-24-0088.1

© 2025 American Meteorological Society. This published article is licensed under the terms of the default AMS reuse license. For information regarding reuse of this content and general copyright information, consult the AMS Copyright Policy (www.ametsoc.org/PUBSReuseLicenses).

Unauthenticated | Downloaded 04/10/25 01:22 AM UTC

forecasting models and our understanding of the global water cycle. TRMM was equipped with a precipitation radar, a microwave imager, and a visible and infrared scanner, allowing it to measure rainfall intensity distribution. The GPM mission, which succeeded the TRMM, has shown improved precipitation retrievals on the TP. Xu et al. (2017) highlighted the superiority of the GPM compared to the TRMM for the southern TP region. Other studies have also confirmed that the GPM is better than the TRMM for a larger extent of the southern TP (Li et al. 2019; Xu et al. 2017) and in other mountain ranges (Chiaravalloti et al. 2018; Zhang et al. 2018).

The Integrated Multi-satellitE Retrievals for Global Precipitation Measurement (GPM) (IMERG) provides the highest spatial (0.1°) and temporal (30 min) resolutions before this study, which has a high potential for hydrometeorological applications in the YGC region. Previous studies have recommended that further improvement of the precipitation retrieval algorithm is required to consider the topographic influences for the GPM precipitation products (Arshad et al. 2021; Li et al. 2023; Xu et al. 2017). The performance of the IMERG strongly depends on the topography (Arshad et al. 2021; Li et al. 2023) and precipitation intensity (Kazamias et al. 2022; Xu et al. 2017). Fang et al. (2019) reported that more studies are still needed to validate IMERG data in regions with complex topography. O and Kirstetter (2018) showed that the precipitation in high-elevation regions may be underestimated by IMERG. There are concerns regarding the errors associated with IMERG over the TP. Several studies have focused on the error characteristics of the IMERG estimates for the TP region. Li et al. (2022) reported that the bias of the annual amount of precipitation (frequency) of the IMERG for the TP region is approximately 10% (20%). Kumar et al. (2021) reported that satellite-based gridded precipitation products capture the seasonal and diurnal cycles and recommended that the IMERG be used for hydroclimatic applications on the eastern TP. Comparatively, Brunetti et al. (2021) verified that the IMERG can be used in landslide early warning systems, particularly in the poorly gauged areas on the southern slopes of the Himalayan Mountains. The IMERG half-hourly precipitation product is useful for studying the precipitation characteristics of the YGC because of its fine spatiotemporal resolution. However, the errors and uncertainties of the IMERG product should be quantified before applying it to hydrological and climate studies in the YGC region.

This study aimed to evaluate the performance of the GPM IMERG V06 Final Run data using a dense rain gauge network established in the YGC in 2018. By leveraging this ground-based data, we sought to assess and calibrate the satellite precipitation products to enhance its accuracy and reliability in this challenging region.

2. Datasets and methodology

a. Study area and in situ data

The YGC is characterized by significant topographic relief and is located in the mountainous region of the southeastern TP (SETP) (Fig. 1a). The YGC is one of the deepest, longest, and most dangerous canyons in the world, with a total length of 496.3 km and maximum depth of 5382 m (Yang and Gao 1996). The YGC runs through a roughly southwest–northeast-trending valley range to the south of 29.5°N. Then, it bends to the southeast–northwest to the north of 29.5°N. The Hengduan Mountains extend from south to north and are located to the east of the YGC. The Himalayan Mountains, with an east–west orientation, are located to the west of the YGC. As moisture is transported from southern Asia to the interior of the TP, the Hengduan, the Himalayas, Namcha Barwa, and Galongla mountains act as barriers to the advance of moisture, which makes the YGC a moisture supply channel for the TP. This is one of the largest moisture transport channels on the TP. The YGC region (29°–30.2°N, 94.7–95.8°E; Fig. 1b) is the most concentrated area of heavy precipitation on the TP. Therefore, investigating the IMERG precipitation product may offer unique insights that are useful for conducting rainfall studies and/or predictions for this region.

A network of 18 precipitation observation stations was established one after another since November 2018 (+ sign in Fig. 1c). Each station comprised a HOBO tipping-bucket rain gauge with a precision of 0.2 mm. The rain gauge datalogger recorded the time and date for each tip. One tip equals 0.2 mm. It provides the details needed to determine rainfall rates and duration. The gauges were placed 1.0 m above ground level (AGL). Station numbers 1–16 (Table 1) were installed from south to north in the YGC. Stations numbers 17 (Danka) and 18 (Lulang) were located in the Palong Zsangbo Valley and the Yarlung Zsangbo Valley, respectively. There were only a few snowfall events at the two high-altitude stations, Lulang and Danka, during our intensive winter snow observation period in 2021. Snowfall had a limited influence on the accuracy of the rain gauge measurements, and we used the term rainfall throughout this paper. These rain gauge sites formed a transect along the YGC from 750 m above mean sea level (MSL) to approximately 3320 m MSL (Fig. 1b). Table 1 presents the detailed rain gauge station information. The longest dataset covered an approximately 4-yr period from November 2018 to 2022. These observation data were not utilized in the calibration process of the IMERG product. Thus, they were considered independent and used to evaluate and calibrate the hourly precipitation estimate of the IMERG data for the YGC watershed. The YGC region has a strong elevation gradient due to its complex orography, which makes it difficult to visit the remote area. Considering the accessibility and the local environment, two stations (Gelin and Renqingben) were placed on the side peaks of the valley; five stations (Dexing, Yimin, Pailong, Danka, and Lulang) were installed on the valley floor; and 11 stations (Beibeng, Yarang, Motog, Wenlang, Bari, Miri, Linduo, Dongren, Kabu, 80K, and Xironggou) were installed on the valley slopes. A sufficient number of stations within a grid cell were necessary to account for the subgrid variability and obtain a meaningful evaluation of the grid values of the IMERG product. The rain gauge network installed in the YGC was considered useful in this regard. It should be noted that although efforts were made to distribute the stations as evenly as possible, there were natural conditions that limited the locations of the equipment.

Unauthenticated | Downloaded 04/10/25 01:22 AM UTC

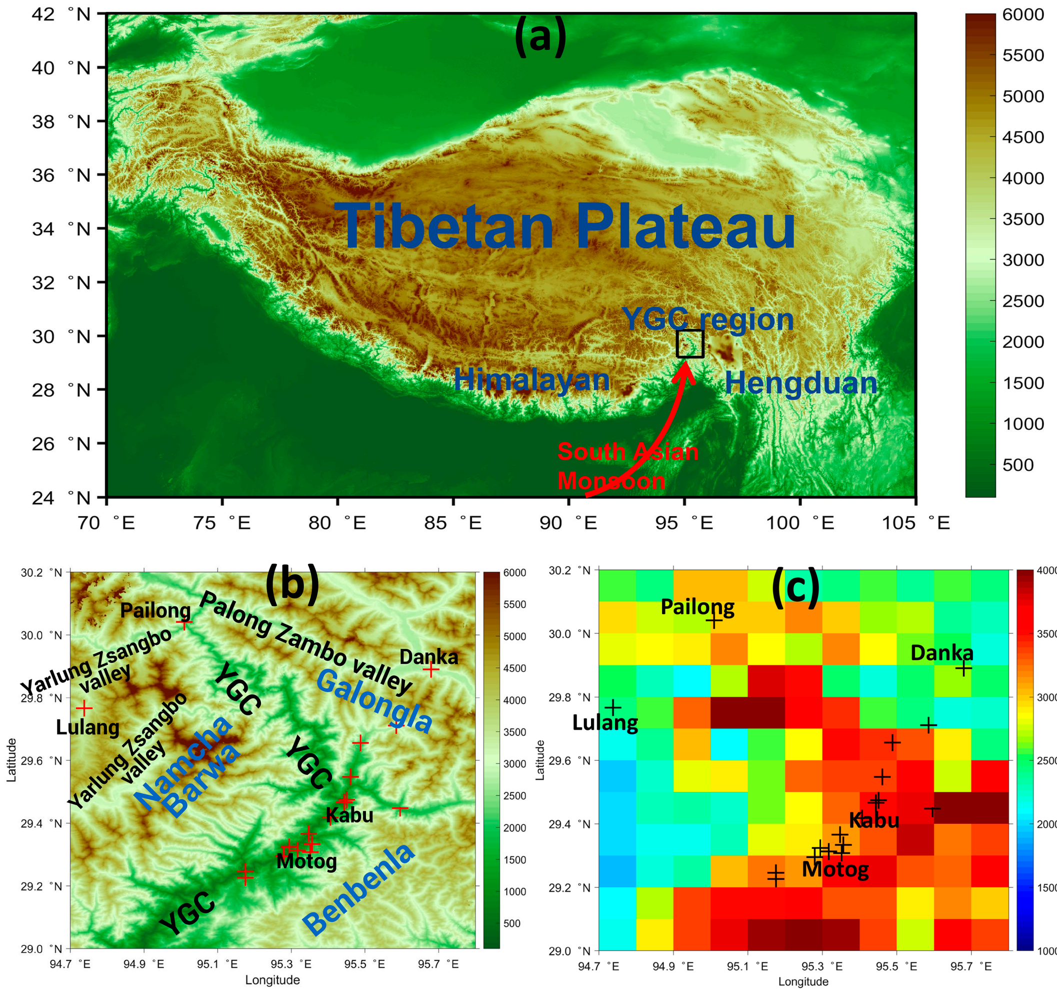

FIG. 1. (a) Location of the YGC region surrounded by the eastern Himalayan and Hengduan mountains; the background color shows an elevation map of the TP (m), (b) the digital elevation map (DEM; m) for the YGC region, and (c) annual number of precipitation events (defined by half-hourly precipitation > 0 mm h^{-1}) in the YGC region retrieved from the IMERG-F dataset. The locations of the rain gauges along the YGC are denoted by the plus sign.

b. GPM satellite precipitation data

In recent years, high-resolution satellite precipitation estimates have been widely used to study the fine-scale structures and properties of precipitation systems. Given the heterogeneity of the spatial distribution of the precipitation in the YGC due to the large elevation difference, the spatial and temporal resolutions of the precipitation data products, such as the Global Precipitation Climatology Centre (GPCC) (Schamm et al. 2014), TRMM Multisatellite Precipitation Analysis (TMPA) (Meng et al. 2014), and Asian Precipitation–Highly Resolved Observational Data Integration Towards Evaluation of Water Resources (APHRODITE) (Yatagai et al. 2012), are relatively coarse compared to the cross-valley spatial scale of the YGC and thus are unable to reflect detailed precipitation variations in the YGC. IMERG has the advantage of 0.1° resolution, which is closer to the cross-valley scale and permits it to be used for resolving precipitation variations in the YGC. One additional advantage of the IMERG product is its high temporal resolution (30 min) which allows it to be used for resolving the diurnal variations in precipitation, furthering our understanding of regional weather processes (Liu et al. 2019). The dual-frequency precipitation radar of the GPM has a higher sensitivity for light precipitation (Casella et al. 2017; Xu et al. 2017). The IMERG product is based on the unified U.S. algorithm and constitutes a multisatellite precipitation product (Huffman et al. 2019). The GPM system provides an initial quick estimate that is successively improved as additional data are made available. The final step utilizes monthly gauge data to create research-level products, IMERG Final Run product. Cumulative distribution matching method was not used in the Final Run product.

In this study, we used the GPM IMERG V06 level 3 Final Run precipitation product with high resolutions (0.1° and 30 min). This final product (GPM_3IMERGHH.06) was downloaded from online (https://gpm1.gesdisc.eosdis.nasa.gov/data/GPM_L3/). It is a research-level product. This product is a combination of microwave and infrared satellite data.

Unauthenticated | Downloaded 04/10/25 01:22 AM UTC

TABLE 1. The information of rain gauge sites. Light (<10 mm day^{-1}), moderate (10–25 mm day^{-1}), and heavy rainfall (≥ 25 mm day^{-1}).

			Location			IMERG-F MB (IMERG-F minus rain gauge) (mm day^{-1})			IMERG-F-CDF MB (IMERG-F-CDF minus rain gauge) (mm day^{-1})		
No.	Site name	Elevation (m)	Lat (°)	Lon (°)	Observation period	Light	Moderate	Heavy	Light	Moderate	Heavy
1	Beibeng	853	29.245	95.175	November 2018–2022	−0.87	−0.22	7.30	0.18	−0.32	5.91
2	Gelin	1789	29.226	95.175	April 2020–November 2022	−0.80	−1.10	4.53	0.25	−1.20	3.12
3	Yarang	757	29.295	95.279	November 2018–2022	−0.88	−1.66	2.99	0.11	0.14	4.16
4	Motog	1300	29.312	95.317	November 2018–April 2021	−0.66	−1.22	3.54	0.33	0.58	4.70
5	Dexing	737	29.324	95.294	November 2018–2022	−0.77	−1.28	4.95	0.22	0.53	6.12
6	Wenlang	1245	29.366	95.340	November 2018–2022	−0.90	−1.98	3.06	−0.12	−0.89	2.37
7	Bari	1700	29.333	95.356	June 2020–April 2022	−0.75	−1.27	3.16	0.12	−0.37	3.67
8	Renqingben	2058	29.307	95.351	June 2020–November 2022	−0.81	−0.11	2.14	0.06	0.79	2.66
9	Miri	832	29.418	95.406	November 2018–April 2022	−0.86	−0.55	2.28	0.12	−0.36	4.96
10	Linduo	840	29.466	95.443	June 2020–April 2022	−1.00	−1.83	−3.24	0.03	−0.66	−4.60
11	Dongren	1185	29.547	95.461	November 2018–April 2021	−0.79	−1.62	4.84	0.28	−0.94	−0.58
12	Kabu	1425	29.473	95.451	November 2018–2022	−1.20	−1.27	9.16	−0.14	−0.59	3.73
13	Yimin	1751	29.448	95.596	June 2020–November 2022	−0.56	−1.22	11.02	0.76	−0.18	9.29
14	80K	2109	29.656	95.488	November 2018–2022	−1.75	−1.39	7.52	−0.73	−0.17	3.55
15	Xironggou	2786	29.710	95.585	November 2018–2022	−1.79	−2.03	1.92	−0.52	−0.83	−3.04
16	Pailong	2081	30.041	95.009	May 2019–March 2022	−1.13	−0.13	8.71	0.34	0.83	2.64
17	Danka	2700	29.890	95.680	November 2018–April 2022	−0.94	−0.95	3.46	0.15	0.39	2.16
18	Lulang	3328	29.766	94.748	November 2018–April 2022	−0.36	1.56	7.51	0.87	0.97	7.46
			Mean			−0.93	−1.02	4.71	0.13	−0.13	3.24

Unauthenticated | Downloaded 04/10/25 01:22 AM UTC

All sensor precipitation products were intercalibrated to Combined Radar-Radiometer Algorithm (CORRA) for both the TRMM and GPM eras and climatologically calibrated to monthly estimates of the Global Precipitation Climatology Project (GPCP) (Huffman et al. 2019). The final product includes data fields for the precipitationCal, HQprecipitation, IRprecipitation, and IRkalmanFilterWeight variables. The precipitationCal is a multisatellite precipitation estimate with gauge calibration that is recommended for general use and is denoted as the IMERG-F in this paper. The HQprecipitation data provide a merged microwave (MW)-only precipitation estimate, and the IRprecipitation is an infrared (IR)-only precipitation estimate. Both the HQprecipitation and IRprecipitation were used with the Kalman filter to produce the final IMERG product. We also used the HQprecipitation (denoted as GPM-MW) and IRprecipitation (GPM-IR) to diagnose the source of error of the IMERG-F.

Both IMERG-F and rain gauge data were preprocessed to be hourly accumulated precipitation, and then they are compared and evaluated. Daily, monthly, and annual precipitations were further derived from the hourly accumulated precipitation. Hourly rainfall frequency is derived as the ratio of the number of hourly rainfalls > 0 mm h^{-1} to the total number of hourly rainfalls ≥ 0 mm h^{-1} during one specific hour. Hourly rainfall rate is the mean value of hourly rainfall rate ≥ 0 mm h^{-1}. Monthly rainfall frequency is derived as the ratio of the number of hourly rainfalls > 0 mm h^{-1} to the total number of hourly rainfalls $\geq$ 0 mm h^{-1} in each month. Monthly rainfall rate is the mean value of hourly rainfall rate ≥ 0 mm h^{-1} in that month.

c. *CDF bias calibration and evaluation metrics*

Proper assessment of the IMERG-F could have impacts on the improvement of the precipitation retrieval algorithm in complex mountainous areas. Before using it for further analysis, the IMERG-F was evaluated in terms of its ability to reflect the observed precipitation characteristics. The coordinates of the gauges were used to extract the corresponding IMERG-F and GPM-IR precipitation time series for comparisons. Then, a bias removal method, cumulative distribution function (CDF) matching, was used to calibrate IMERG-F. The CDF-calibrated IMERG-F was denoted as IMERG-F-CDF in this paper.

CDF matching method was often used in bias correction, for example, to calibrate satellite soil moisture (Reichle and Koster 2004). This method calibrates the bias through matching simulated/estimated data distributions to observational data, ensuring their consistency in probability distributions. By comparing the CDFs of observed and simulated/estimated datasets, systematic biases in model predictions can be corrected. This method can also improve accuracy in predictions across different data ranges. We used this calibration method to match the CDF of the satellite to that of the rain gauge data. The code for CDF bias calibration of IMERG-F can be found at GitHub (https://github.com/TSEBS/CDF-mating-of-GPM-IMERG-to-rain-gauge/tree/main). The CDF correction method is based on the statistical distribution. More rain gauge data sample will represent real statistical distribution and benefit accuracy of the correction. Hereby, each gauge was compared to the grid box in which it falls, regardless of the presence of other gauges.

The IMERG-F dataset's time labels were adjusted to match Beijing standard time (BST), which is 8 h ahead of Greenwich mean time (GMT). Various indicators (general statistical indices, rainfall intensity classification indicators, and probability distribution function) were adopted as metrics to evaluate the IMERG-F precipitation product. Daily precipitation was classified into daily light rainfall ($<$10 mm day^{-1}), daily moderate rainfall (10–25 mm day^{-1}), and daily heavy rainfall ($\geq$25 mm day^{-1}). Hourly light rainfall is defined as hourly rainfall below 0.9 mm h^{-1}, and hourly heavy rainfall means which is higher than 0.9 mm h^{-1}. These intensity definitions at hourly and daily temporal scales help us to accurately assess IMERG-F performance in the frequencies and intensities of the daily and hourly rainfall estimations. A probability density/distribution function (PDF) was adopted to check the improvement of the calibrated IMERG-F precipitation. The same number of valid data samples from the rain gauge and IMERG-F datasets was utilized when we compared their averaged diurnal and monthly variations and PDFs. The hourly value of the IMERG-F was set to "nan" if the rain gauge site had an invalid value due to a shortage of battery power or other errors.

3. Results

a. *IMERG-F underestimates hourly rainfall frequency and rate*

The evaluation of the satellite product at subdaily time scales in the YGC has many implications. The IMERG-F product can approximately reproduce the diurnal cycles of the observed hourly rainfall frequency and rate (Fig. 2). However, it underestimated the hourly rainfall rate and frequency. O and Kirstetter (2018) also reported that IMERG-F tends to underestimate the diurnal variations over the mountainous regions in the western and eastern United States. IMERG-F is a combination product of GPM-MW and GPM-IR (Adler et al. 2003), which combination has been calibrated with rain gauge observations from GPCC to produce IMERG-F. Our previous study has compared the GPCC calibrated, uncalibrated, GPM-MW and GPM-IR precipitation against the rain gauge observations in the YGC (Li et al. 2023). It demonstrated that GPM-MW and GPM-IR have more serious lower estimation than IMERG-F. The correction of merged GPM-MW and GPM-IR using GPCC can only partly solve the low estimation of GPM-MW and GPM-IR. This is due to that only two rain gauge sites in the YGC region have been used to do the calibration. These findings necessitate this study to provide a solution for address the serious lower estimation in the YGC.

YGC is a complex mountainous region, and most of the highest peaks in this region are covered by snow and ice sheet. The snow and ice cover on the peaks prevent the use of GPM microwave observations in the YGC. This makes GPM-MW has a low percentage of valid data in the YGC region, and it is unreliable to analyze its probability density distribution. Hereby, we mainly demonstrate the results of IMERG-F and GPM-IR in this study.

Unauthenticated | Downloaded 04/10/25 01:22 AM UTC

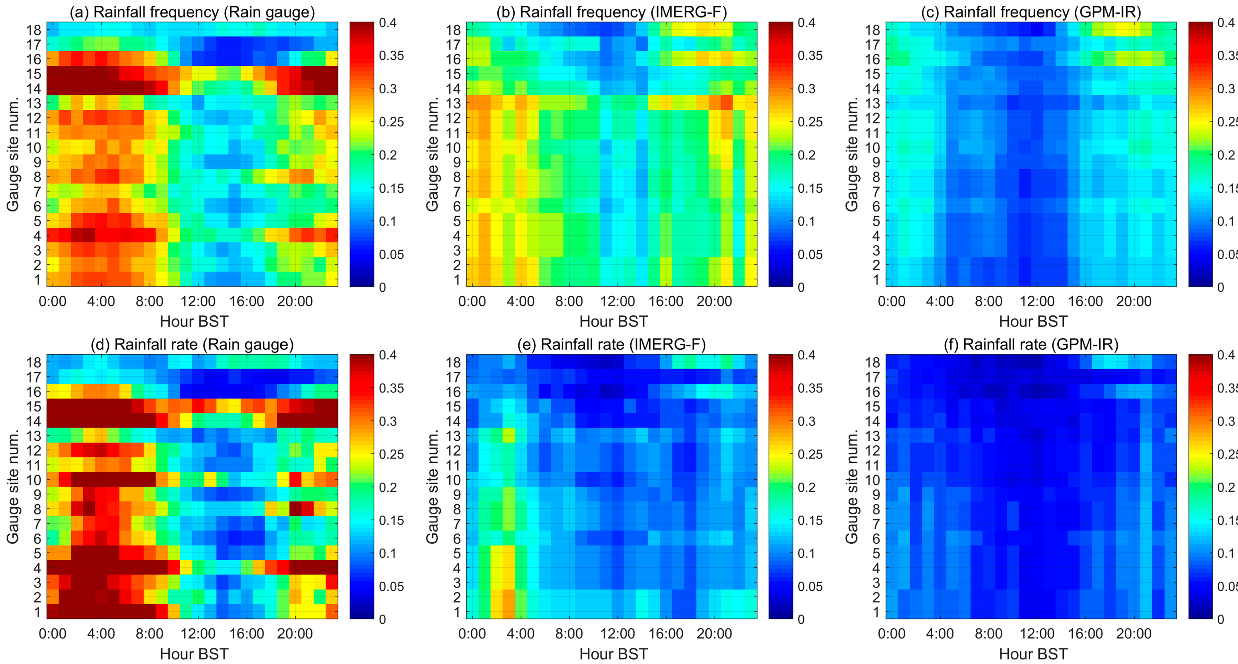

FIG. 2. (a)–(c) Hourly rainfall frequency and (d)–(f) hourly rainfall rate (mm h^{-1}) derived from (a),(d) the rain gauges, (b),(e) IMERG-F, and (c),(f) GPM-IR datasets. The site number and its corresponding site name are listed in Table 1.

Figure 2 shows that GPM-IR has a more serious underestimation than its merged product IMERG-F. It is initially unclear whether the underestimation was caused by light or heavy precipitation. The PDF analysis results in Fig. 3 could help us to address this question. Figure 3a compares the probability density of the hourly precipitation for the rain gauge, IMERG-F, and GPM-IR datasets. The IMERG-F had much higher probability than the observations for hourly light rainfall (<0.9 mm h^{-1}), but it had lower probability for hourly heavy rainfall (in the range of 0.9–5.0 mm h^{-1}). This indicates that the IMERG-F contained too many hourly light rainfall events and too few hourly heavy rainfall events in the YGC region. To improve the quality of the IMERG-F rainfall estimation in this region, the light hourly rainfall occurrence should be suppressed and the heavy hourly rainfall occurrence should be increased.

The GPM-IR had a more serious problem than the IMERG-F. The higher occurrence of light rainfall and low occurrence of heavy rainfall of GPM-IR were out of our expectation. It is easier for IR to capture heavy rainfall with high and cold cloud tops but difficult for IR algorithms to correctly capture warm rain clouds, which tend to produce light rainfall. However, here it shows that the IR algorithm seems to capture more light rainfall but missed heavy rainfall. Figure 2 shows that the heavy rainfall in the YGC mostly happens in the nighttime. Heavy rainfall clouds in the nighttime are not caused by deep convection. The cloud top for heavy rainfall in the nighttime of the YGC is not high. Chen et al. (2017) also reported that the cloud-top height on the south slope of the Himalayas is lower than that of flat Gangetic Plains and Tibetan Plateau. The lower cloud top could explain why GPM-IR has missed observation of heavy rainfall. Another explanation is that the rainfall cloud in the YGC was dominated by a two-layered vertical structure (Zhou et al. 2021). The GPM-IR satellites cannot acquire information of the two-level clouds. This makes GPM-IR have difficulty in capturing the signal from the lower clouds, which causes GPM-IR miss catching of heavy rainfall and overestimation of the light rainfall in the YGC region.

To analysis the influence of above hourly rainfall bias on the daily rainfall amount estimation, we also show the probability density of daily rainfall in Fig. 3b. Daily rainfall produced a similar PDF as that of the hourly rainfall. For the daily amount of rainfall, the IMERG-F and observations had maximum probability density at 2.9 and 6.6 mm day^{-1}, respectively. The daily rainfall of the IMERG-F had a higher probability than that of the observations except for rainfall rates of greater than 10 mm day^{-1}. The probability density of daily rainfall demonstrated that IMERG-F overestimates the daily light rainfall (<10 mm day^{-1}) frequency and underestimates the frequency of daily rainfall higher than 10 mm day^{-1}. This means that IMERG-F contained too many daily light rainfall events and too few daily heavy rainfall events at daily temporal scale in the YGC region.

The IMERG-F exhibited a relative flatter diurnal variation pattern, compared to that of the rain gauges (Figs. 3c,d). The IMERG-F underestimated the diurnal variations in the rainfall frequency and rainfall rate. The mean rainfall frequency of the IMERG-F was approximately 18%, which was slightly lower than the 23% frequency derived from the rain gauge observations. The mean rainfall rate of the IMERG-F was approximately 0.11 mm h^{-1}, and the value for the rain gauge was approximately 0.22 mm h^{-1}. GPM-IR and IMERG-F

Unauthenticated | Downloaded 04/10/25 01:22 AM UTC

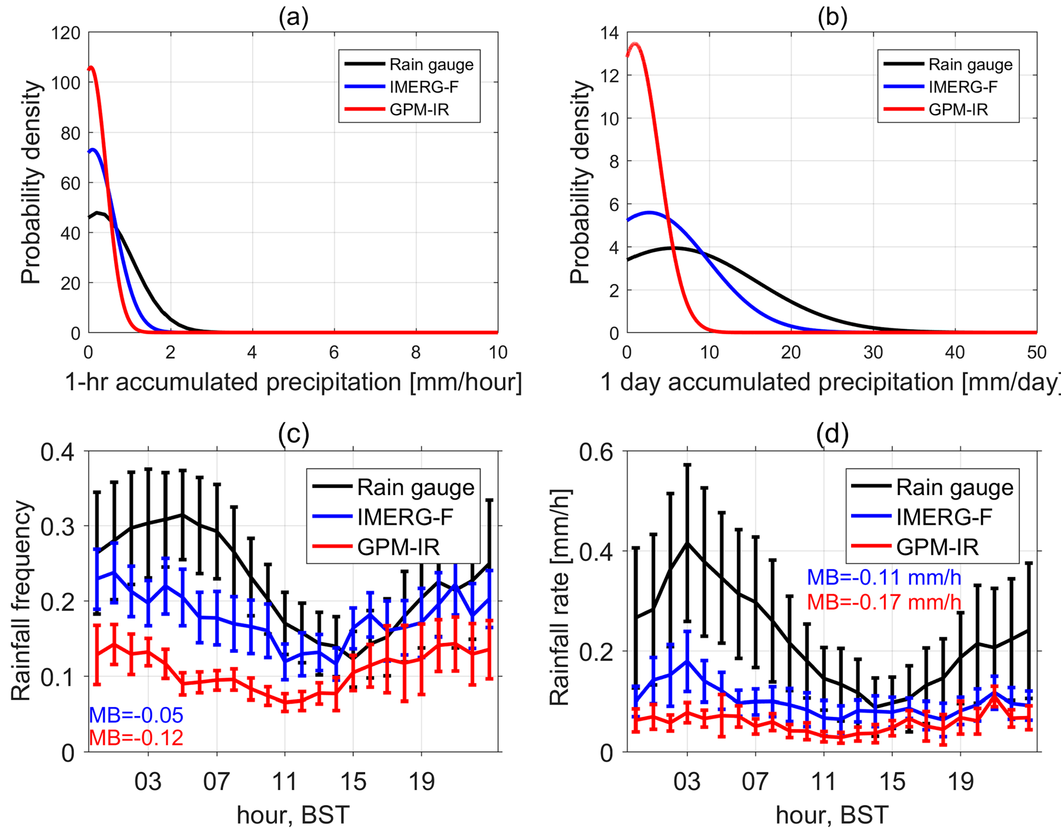

FIG. 3. PDFs of the (a) hourly rainfall and (b) daily rainfall from the IMERG-F, GPM-IR, and rain gauge observations in the YGC region. (c),(d) The median diurnal variations of the rainfall frequency and rainfall rate at the rain gauge sites, respectively. The lengths of the vertical error bars in (c) and (d) are two standard deviations. The local solar time in the YGC is about 2 h later than BST. All the rain gauge stations were used to calculate the average values in this figure.

hourly rainfall rate has a mean bias (MB) of -0.17 and -0.11 mm h^{-1} against rain gauge measurement. Their hourly rainfall frequency also has a negative mean bias of -0.12 and -0.05, respectively. Hereby, IMERG-F has a lower-estimation problem of the hourly rainfall rate and frequency. GPM-IR has more serious lower-estimation problem than IMERG-F. Both the lower frequency and lower rainfall rate were the factors causing the underestimation of accumulated daily and monthly rainfall, which was demonstrated below.

Meanwhile, the IMERG-F was able to capture the early-morning peak of the rainfall rate and the afternoon valley of the rainfall frequency in the gauge observations. This indicates that the IMERG-F has a potential to capture the diurnal variations of the rainfall frequency and the rainfall rate, after a calibration. Late night and early morning have a higher frequency and intensity than other time. The rainfall frequency and rate during late night and early morning were more seriously underestimated by IMERG-F than other time. A statistical calibration method which could increase the heavy rainfall rate and frequency in the late night and early morning will be an effective solution for the lower estimation in this region.

To check the performance of IMERG-F in seasonal variation, we compared the monthly rainfall amount, monthly rainfall frequency, and monthly rainfall rate. A dry bias was found in the IMERG-F in terms of the accumulated monthly precipitation (Fig. 4a). IMERG-F underestimates the monthly rainfall frequency and rate. The absolute bias of monthly amount was larger in the summer months than in the other months. However, the contribution of each month's rainfall to the annual precipitation exhibited a high consistency with that of the ground-based estimates (Fig. 4b). Thus, the underestimation of annual rainfall can be evenly distributed over the months when calibrating the IMERG-F precipitation data for the YGC region. Monthly IMERG estimation was nearly a constant scale factor times that of the gauges (Fig. 4b). This might be a fact showing what GPCP calibrations have done to the IMERG.

b. *The physical explanation of the bias source*

The 16 stations in the YGC demonstrated that the IMERG-F had a dry bias with varying degrees, but this was not observed at the two sites, Danka and Lulang. Two rain gauge sites of China Meteorological Administration (CMA) were located in the same GPCC grid of Danka and Lulang [please refer to Fig. 1 in Li et al. (2023)]. It was confirmed from GPCC that both CMA sites have been considered in production

Unauthenticated | Downloaded 04/10/25 01:22 AM UTC

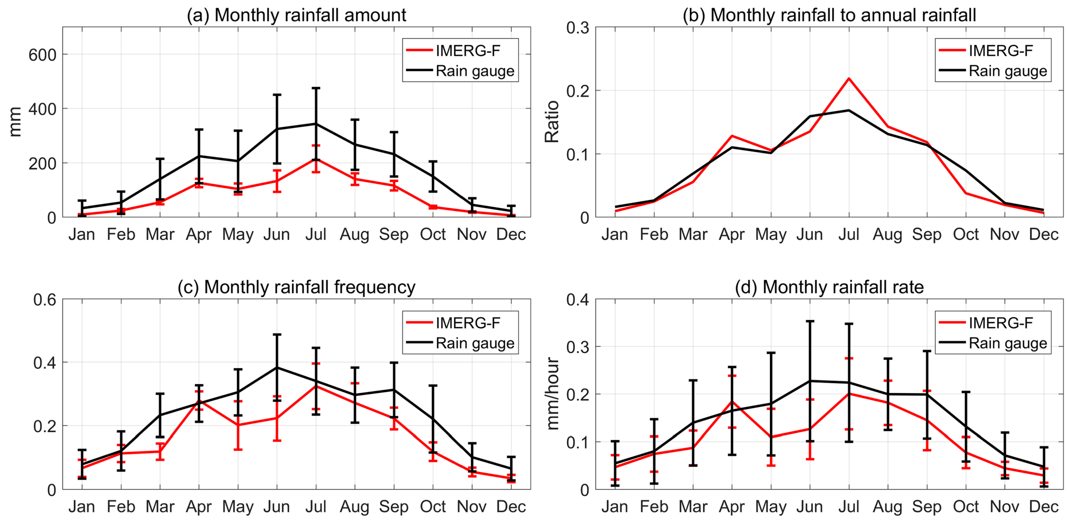

FIG. 4. (a) Monthly rainfall, (b) ratio of monthly to annual rainfall, (c) monthly rainfall frequency, and (d) monthly rainfall rate for the IMERG-F and in situ rain gauges. The ratio of the monthly rainfall to the annual rainfall was calculated using the monthly rainfall values in (a). The lengths of the vertical error bars in (a), (c), and (d) are two standard deviations. All the rain gauge stations were used to calculate the average values in this figure.

of the GPCC product. GPCC data have been used by GPM scientists to calibrate the IMERG-F. Hereby, the two CMA sites were already used to calibrate the IMERG-F grid of Danka and Lulang stations located in. It becomes natural that no dry bias was observed at Danka and Lulang in this study.

The IMERG-F product tended to underestimate precipitation in the YGC Valley. Our previous study indicated that GPM-MW also has underestimates in the YGC. We checked to determine whether the GPM-MW underestimation was due to the ground echo from the mountains around the rain gauge site, which could have been misidentified as the melting layer in a stratiform cloud. The freezing level derived from the microwave radiometers of the TP-PROFILE at Motog, Kabu, and Lulang (Chen et al. 2024b) is analyzed in Fig. 5. The results revealed that the highest frequency of the melting layer occurred at 1.5 km above the ground level at Motog, at 3.0 km over Kabu, and at 2.5 km over Lulang. The YGC rain gauges stations are located in valleys with depths of 0.5–3.5 km. Most of the freezing levels observed at the three sites were within the height range of the surrounding mountains. This explains why the high peaks of the YGC were covered by snow and ice, and GPM-GW cannot fully work in this area. The ground echo from the surrounding mountains has a high chance to be taken as freezing levels by GPM-MW. Cloud particles start melting and evaporating below the freezing level. Hereby, the fake melting layer due to mountain ground echo will lead to the lower estimation of GPM-MW precipitation. It was deduced that the misidentification of the freezing level due to ground echo may be the reason for the underestimation of GPM-MW in the YGC.

In fact, two layers of clouds were often observed in the YGC Valley (Chen et al. 2017; Zhou et al. 2021). Zhou et al. (2021) observed two peaks of cloud-base height located at 0–1 km and 2–3 km using a ground-based Ka-band cloud radar at Motog, which was established by an INVC project (Chen et al. 2024a). The low clouds at 0–1 km correspond to precipitation clouds, and the upper-level clouds at 2–3 km are nonprecipitable clouds (Zhou et al. 2021). Lower-level orographic stratus clouds often cap the hills and small mountains on the sides of the YGC Valley. In addition, upper-level clouds homogeneously covered a large area. IR satellites use the brightness temperature to retrieve cloud-top features (temperature and albedo) rather than directly estimating the surface precipitation. Within GPM-IR precipitation retrieval algorithm, cloud-patch features are extracted at three separate temperature levels (220, 235, and 253 K), which are chosen to represent the cloud patches at different altitudes in the atmosphere (Huffman et al. 2019). Precipitation is assigned to each classified cloud-patch

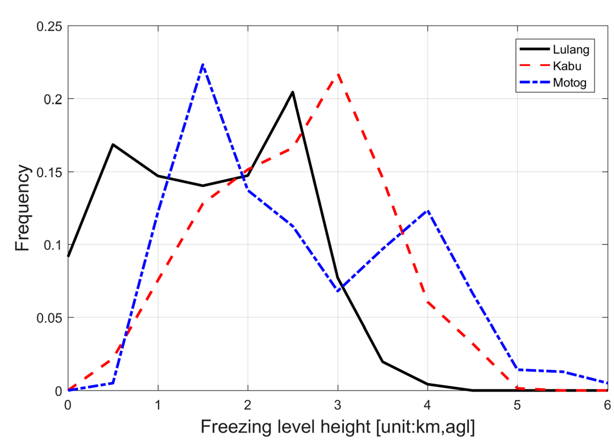

FIG. 5. Histogram of the freezing level height (km) at the Lulang, Kabu, and Motog rain gauge sites.

Unauthenticated | Downloaded 04/10/25 01:22 AM UTC

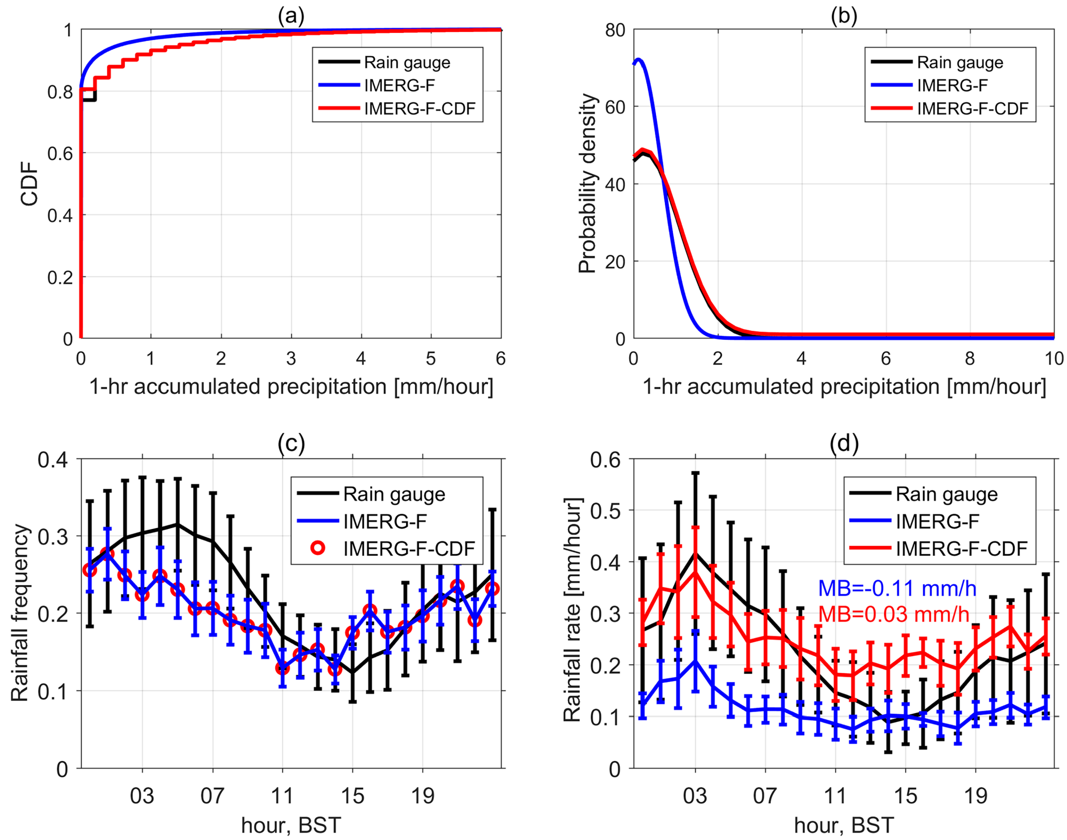

FIG. 6. Comparison of (a) CDFs and (b) PDFs of the 1-h accumulated rainfall derived from the IMERG-F, IMERG-F-CDF, and the 18 rain gauge observations in the YGC region. (c),(d) The median diurnal variations of the rainfall frequency and rainfall rate of the 18 rain gauge sites, respectively. The lengths of the vertical error bars in (c) and (d) are two standard deviations. The local solar time in the YGC is about 2 h later than BST.

group. The two-layer clouds tell us that the surface precipitation is decoupled from the cloud top. The GPM-IR satellite cannot acquire information about the lower-level clouds in the YGC. This affects the IR estimates. GPM is largely unable to retrieve microwave signals of precipitation, due to the snow or ice covers in the mountain peaks in the YGC region. When the lower cloud layer is mostly liquid, this also affects the microwave estimates. Insufficient microwave sources can lead to wide discrepancies in the IMERG estimates (O and Kirstetter 2018). This makes it difficult for the IMERG-F to capture the two layers of cloud in the YGC. These may be the reason for the underestimation of the GPM-IR and IMERG-F in the YGC region. It should be noted that these explanations of two-layer clouds leading to the IMERG-F underestimation need further investigation.

In addition, the ice particle size distribution in the GPM IMERG algorithm for the YGC region might differ from that observed by Xu et al. (2023b). Uncertainties in the ice particle size distribution can also lead to underestimation of MW satellite precipitation. Therefore, future research should intensify observations of cloud microphysics characteristics within the YGC region (i.e., Xu et al. 2023a) to formulate a specific ice particle spectral parameter tailored to its conditions.

c. *CDF reduction of the IMERG-F underestimation*

IMERG-F underestimates the rainfall frequency and rate at both the daily and monthly scales. To address the underestimations, the CDF calibration method was applied to the IMERG-F hourly rainfall. Figure 6a shows the CDF of data from the rain gauge, IMERG-F, and IMERG-F-CDF. IMERG-F-CDF has a cumulative distribution curve closer to that of the rain gauge than that of IMERG-F. CDF calibration makes the PDF curve of IMERG-F close to that of the rain gauge (Fig. 6b). In addition, the CDF calibration method significantly increased the satellite rainfall rate (Fig. 6d) and rarely changed the rainfall frequency (Fig. 6c). The mean bias of hourly rainfall rate for IMERG-F was decreased from -0.11 to 0.03 mm h^{-1}. Figure 7 compares the effects of CDF calibration on the averaged hourly rainfall at each site. It demonstrates that the lower estimation of hourly rainfall rate at the most sites has been improved.

The improvement of different intensity of daily rainfall (light, moderate, and heavy rainfall) is listed in Table 1. The frequencies of the three intensities from the IMERG-F and IMERG-F-CDF were compared against that of the in situ observations (Fig. 8). Table 1 shows that IMERG-F underestimated the intensity of daily light (<10 mm day^{-1}) and moderate rainfall (10–25 mm day^{-1}) and overestimated the

Unauthenticated | Downloaded 04/10/25 01:22 AM UTC

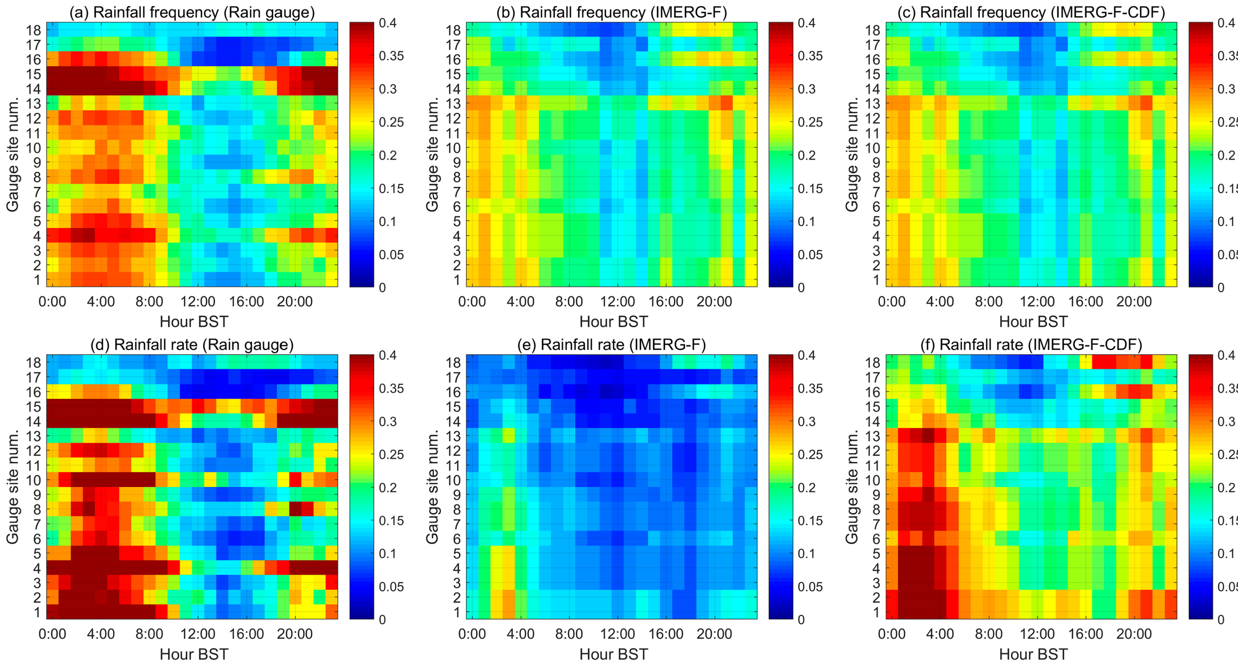

FIG. 7. (a)–(c) Hourly rainfall frequency and (d)–(f) hourly rainfall rate (mm h^{-1}) derived from (a),(d) the rain gauges, (b),(e) the IMERG-F, and (c),(f) the IMERG-F-CDF datasets. The site number and its corresponding site name are listed in Table 1. The local solar time in the YGC is about 2 h later than BST.

heavy rainfall (≥25 mm day^{-1}) intensity. The bias of light, moderate, and heavy daily rainfall intensity was decreased by CDF from −0.93, −1.02, and 4.71 to 0.13, −0.13, and 3.24 mm day^{-1}, respectively. Meanwhile, the frequency of light daily rainfall was overestimated, and the frequency of moderate and heavy daily rainfall was underestimated (Fig. 8). The bias of light daily rainfall frequency was decreased from 0.31 to 0.01. The bias of moderate and heavy daily rainfall frequencies decreased from −0.19 and −0.13 to 0.002 and −0.006, respectively. Figure 8 demonstrates the effectiveness of CDF calibration on the improvement of IMERG-F frequencies of the different daily rainfall intensities. CDF calibration has improved the frequency and intensity estimation of IMERG-F for the three daily rainfall intensities.

These figure results confirmed that IMERG-F-CDF has improved the frequency and intensity estimation of hourly and daily rainfall. A better performance of IMERG-F-CDF than IMERG-F at monthly temporal scale is also confirmed in Fig. 9. The mean bias of monthly rainfall was decreased from −95.0 to −5.2 mm $month^{-1}$ by the CDF calibration (Fig. 9). There are two sites (80K and Xironggou) that still have an underestimation problem after the CDF calibration. This is due to severe underestimation by the original IMERG estimates at these two sites. These two sites are more cline to be snowy surface in the winter. The GPM microwave estimates are systematically dropped when the snow product flags these locations as a snowy/icy surface. The CDF bias was computed for the entire rain gauge observation period. These explain why the CDF calibration does not solve the highly underestimation at these two locations.

The rain gauge data showed that the daily light rainfall days had a frequency of approximately 0.5, while the IMERG-F daily light rainfall had a frequency of 0.8. This comparison revealed that more light precipitation events occurred in the IMERG-F than in the gauge data. One reason for this misidentification was already reported in the TRMM precipitation retrievals, i.e., a ground echo could be misidentified as a melting layer of a stratiform cloud system because the freezing level extends to the surface over the TP (Fu and Liu 2007). Meanwhile, our above analysis of the freezing level has verified that ground echoes from the hills surrounding the YGC rain gauge sites cannot explain more light precipitation problem in the IMERG-F. For both the IMERG and gauge data, the heavy rainfall frequency was much lower than those of the light and moderate rainfall frequencies. The moderate and heavy rainfall frequencies for the IMERG-F were lower than that of the rain gauge data. The higher frequency of light rainfall and the lower frequency of heavy rainfall at daily scale are consistent with the results at hourly scale shown in Fig. 3. This explains that the dominant error source producing the dry biases in the IMERG-F in the YGC region is due to the lower frequencies of the moderate and heavy rainfall. Both the higher frequency of light rainfall and lower frequency of moderate and heavy rainfall included in IMERG-F have been improved by the CDF calibration. That is why the CDF can overcome the dry bias included in the IMERG-F.

4. Conclusions and discussion

Precipitation studies over the YGC mountainous areas rely strongly on satellite precipitation products. One of the key

Unauthenticated | Downloaded 04/10/25 01:22 AM UTC

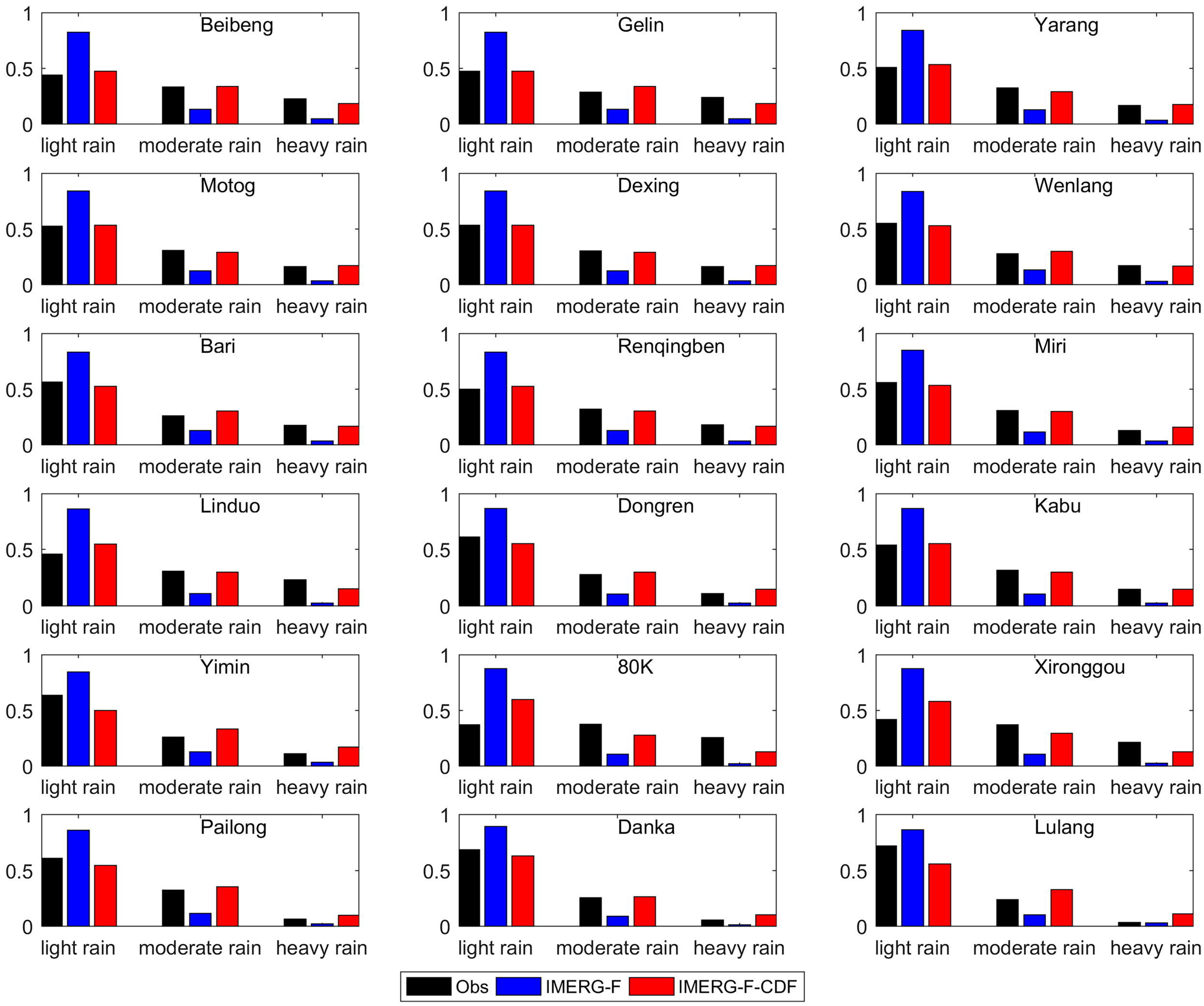

FIG. 8. The frequency of daily light (<10 mm day^{-1}), daily moderate (10–25 mm day^{-1}), and heavy rainfall (≥25 mm day^{-1}) derived from the daily rainfall of the IMERG-F, IMERG-F-CDF, and in situ rain gauges.

challenges for satellite precipitation retrieval algorithm developers is to improve the ability to detect very light/heavy rainfall events, rainfall over topographical regions, and differentiating the rainfall from snowfall (Sunilkumar et al. 2019). The YGC is an ideal testbed for verifying the performance of IMERG in these three aspects. The performance of the IMERG V06 Final Run data was evaluated and compared with a newly installed network of rain gauges in the YGC. The precipitation frequency of the IMERG-F hourly rainfall was generally lower than that of the gauge data. The amount of precipitation from the IMERG-F in the YGC commonly exhibited a dry bias. Kazamias et al. (2022) reported that IMERG V06B Final Run product underestimates the daily rainfall over the western part of Greece, due to satellite sensors' failure to detect the magnitude of orographic rainfall. The misidentification of the freezing level may also be one reason for the underestimation in the YGC region. IMERG-F contained too many hourly light rainfall events and too few hourly heavy rainfall events in the YGC region. One potential source of these errors is the averaging process of GPM-MW and GPM-IR within the Kalman filter used in the IMERG V06 algorithms. As noted by Tan et al. (2021), this averaging approach tends to suppress high rainfall rates while inflating the frequency of low rainfall rates.

Typically, it is easier for IR to capture rain clouds with high and cold cloud tops, but it is difficult for IR algorithms to correctly capture warm rain clouds, which tend to produce light rainfall. However, this study shows that IR seems to have captured more light precipitation but missed heavy precipitation in the YGC. The heavy precipitation in the YGC usually happens in the nighttime. Heavy precipitation clouds in the nighttime are not caused by deep convection. The cloud tops for heavy precipitation in the YGC are not high. This could be the reason why GPM-IR has missed observation of heavy precipitation. The rain cloud in the YGC was dominated by a two-layered vertical structure (Zhou et al. 2021). The GPM-IR

Unauthenticated | Downloaded 04/10/25 01:22 AM UTC

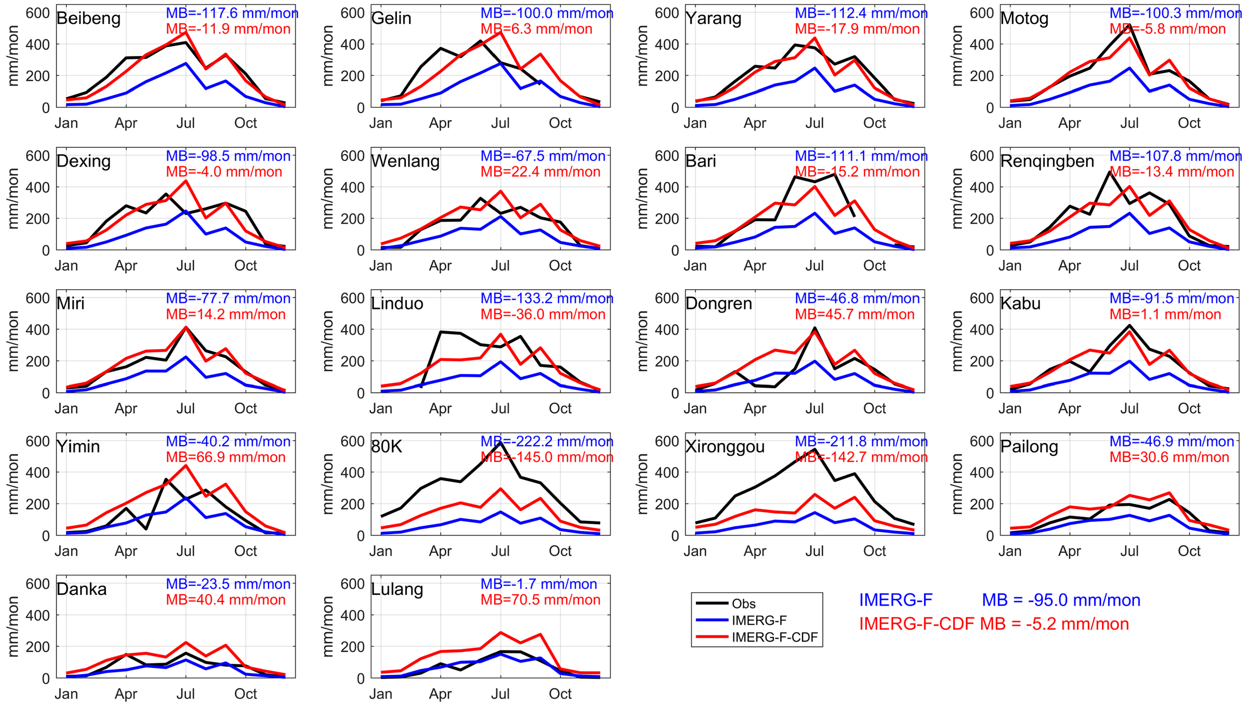

FIG. 9. Monthly rainfall for the IMERG-F, IMERG-F-CDF, and in situ rain gauge estimates (mm month^{-1}).

satellites cannot acquire information of the two-level clouds, which make IMERG-F have difficulty in capturing the precipitation caused by the two-layer clouds in the YGC Valley. This may be another reason why IMERG-F has underestimates of heavy rainfall in the YGC region.

More light precipitation hours appeared in the IMERG-F than in the gauge data. The IMERG-F had a lower occurrence frequency of hourly heavy precipitation, which led to underestimation in the IMERG-F rainfall. This study found that the IMERG-F underestimated the rainfall frequency at the daily and monthly scales. This explains why the monthly and seasonal precipitation amounts were lower than the observations in the YGC region. The IMERG-F has underestimated the light and moderate rainfall intensity and overestimated the heavy rainfall intensity at daily scale. Meanwhile, the frequency of daily light rainfall was overestimated and the frequency of daily moderate and heavy rainfall was underestimated. O and Kirstetter (2018) showed that GPM IMERG V04 Final Run underestimated the orographic and convective precipitation in high-elevation regions. Kazamias et al. (2022) reported that IMERG V06B Final Run product underestimates the daily rainfall over the western part of Greece due to satellite sensors' failure to detect the magnitude of orographic rainfall. The lower occurrence frequency of heavier precipitation from GPM IMERG V06 Final Run in the YGC may also disclose the difficulty of GPM capturing orographic and convective precipitation in the Himalayan Mountain region. The underestimation of the IMERG for intense precipitation events has been also reported in the United States by Tan et al. (2016). Fang et al. (2019) demonstrated that GPM had limited capability to detect extreme rainfall event in regions with complex topography. When using the IMERG-F estimates as input into hydrologic models, the underestimation of the intense precipitation events in the YGC could lead to significant uncertainties in the model outputs. Therefore, the IMERG-F should be used with caution when analyzing and performing model studies on extreme precipitation events in the YGC region.

The CDF-calibrated IMERG-F data can overall reasonably reproduce the observed seasonal and diurnal precipitation patterns. Figure 7 has shown a good result of the CDF calibration. The proposed CDF calibration method might be further applied to GPM-IR to improve its quality.

Our evaluation and calibration of IMERG-F in the YGC region can provide important references for modelers who are using this satellite data to assess global climate model performance for the Himalayan Mountain region. There are other methods available for calibrating the satellite rainfall data. The CDF calibration method primarily focuses on matching the statistical distribution of the data rather than addressing underlying physical processes. While CDF matching can be useful for adjusting the shape and variability of the rainfall distribution, it may not effectively capture localized spatial and temporal variations in precipitation. Another issue with the CDF calibration method is that it can be applied to IMERG-F regardless of whether IMERG-F has the same number of rainfall events as those observed by the rain gauge. It only changes the rate of rainfall events included in IMERG-F, without considering whether this event is real or not.

A critical issue in using a ground-based estimate to assess or improve the accuracy of satellite products is the accuracy of the ground-based estimate. Precipitation records in mountainous areas often face challenges, such as low station density and lack of representativeness, as most of our stations are

Unauthenticated | Downloaded 04/10/25 01:22 AM UTC

located in valleys. The spatial sampling issue is particularly pronounced in places with steep topography.

To address these challenges, we carefully designed the layout of the rain gauge network in the YGC region, aiming to achieve the highest possible station density. However, the region's complex orography, dominated by tall, dense primeval forest, makes regular access and gauge installation difficult. Despite these constraints, three IMERG-F grids in the YGC region are intensively monitored, each with measurements from more than two sites.

For example, the Beibeng and Gelin sites, located within the same IMERG-F grid, have an elevation difference of 936 m, reflecting the grid's topographic complexity. The annual rainfall difference between the two sites is approximately 377 mm yet both recorded monthly rainfall amounts significantly higher than the IMERG-F estimates. Similarly, the Motog, Wenlang, Bari, and Renqingben stations, also in the same grid, have annual rainfall ranging from 1771 to 2292 mm, with an elevation range of 1245–2058 m, and an annual rainfall difference of 521 mm. Like the previous sites, their observed precipitation exceeds the IMERG-F estimates for their grid. Last, the Miri, Linduo, and Kabu stations in another grid show an annual rainfall difference of 143 mm and an elevation difference of 350 m. These three sites also have higher rainfall amount than their matching IMERG-F grid. These findings suggest that the IMERG-F grids, even those with intensive observations, tend to underestimate precipitation in the YGC region. Hereby, the inherent difference between the in situ point observations and satellite area-averaged estimates do not undermine the general conclusions of this study.

Most of the gauges are situated along a deep, narrow valley, with cross-valley scales smaller than a single IMERG grid box. Previous studies have estimated the effective resolution of IMERG to be approximately 40 km (Guilloteau et al. 2021, 2022). This means that IMERG estimates at the validation gauges are likely more representative of the surrounding high terrain. Additionally, the use of GPCC data for calibrating IMERG in the Final Run version explains the higher consistency between IMERG estimates and the observations at the high-altitude stations 17 and 18.

Cloud characteristics also play a role in the observed differences. The cloud-top height on the southern slope of the Himalayas is lower than that over the Gangetic Plains and Tibetan Plateau (Chen et al. 2017). The southern low-elevation area of the YGC region, part of the Himalayan south slope, has lower cloud tops. The northern high-elevation area has higher cloud tops. GPM-IR is more effective at detecting rainfall signals from higher cloud tops, making the northern YGC less biased in IMERG estimates compared with the southern region. These variations in cloud characteristics further explain the observed north–south differences in IMERG-F bias across the YGC region.

In the YGC region, the high spatial variability of the precipitation suggests that more gauges are required to obtain accurate precipitation estimates. The area-averaged precipitation estimates from the rain gauges in this region by this study may have been unrepresentative because the YGC landscape consists of a curved barrier comprising of many small-scale ridges and valleys, and most of the rain gauges are located in valleys for which sufficient information about ridge precipitation is lacking. Hereby, the CDF adjustment in the relative low elevation of the YGC region is somehow not representative of the region as a whole.

Acknowledgments. This research was funded by the National Natural Science Foundation of China (41975009 and U2442213). DC is supported by Tsinghua University (100008001).

Data availability statement. The in-situ rain gauge data for the 18 sites were shared on the repository of the National Tibetan Plateau Data Center. The rain gauge data are available at https://data.tpdc.ac.cn/zh-hans/disallow/ecf7bd52-1e07-4d7b-a185-8e06b07c359a, DOI: https://doi.org/10.11888/Atmos.tpdc.273029. Users can freely obtain the rain gauge data used in this study from the website.

REFERENCES

Adler, R. F., and Coauthors, 2003: The Version-2 Global Precipitation Climatology Project (GPCP) monthly precipitation analysis (1979–present). *J. Hydrometeor.*, **4**, 1147–1167, https://doi.org/10.1175/1525-7541(2003)004<1147:TVGPCP>2.0.CO;2.

Arshad, M., and Coauthors, 2021: Evaluation of GPM-IMERG and TRMM-3B42 precipitation products over Pakistan. *Atmos. Res.*, **249**, 105341, https://doi.org/10.1016/j.atmosres.2020.105341.

Brunetti, M. T., M. Melillo, S. L. Gariano, L. Ciabatta, L. Brocca, G. Amarnath, and S. Peruccacci, 2021: Satellite rainfall products outperform ground observations for landslide prediction in India. *Hydrol. Earth Syst. Sci.*, **25**, 3267–3279, https://doi.org/10.5194/hess-25-3267-2021.

Casella, D., G. Panegrossi, P. Sanò, A. C. Marra, S. Dietrich, B. T. Johnson, and M. S. Kulie, 2017: Evaluation of the GPM-DPR snowfall detection capability: Comparison with CloudSat-CPR. *Atmos. Res.*, **197**, 64–75, https://doi.org/10.1016/j.atmosres.2017.06.018.

Chen, X., D. Cao, Y. Liu, X. Xu, and Y. Ma, 2023: An observational view of rainfall characteristics and evaluation of ERA5 diurnal cycle in the Yarlung Tsangbo Grand Canyon, China. *Quart. J. Roy. Meteor. Soc.*, **149**, 1459–1472, https://doi.org/10.1002/qj.4468.

——, and Coauthors, 2024a: Investigation of precipitation process in the water vapor channel of the Yarlung Zsangbo Grand Canyon. *Bull. Amer. Meteor. Soc.*, **105**, E370–E386, https://doi.org/10.1175/BAMS-D-23-0120.1.

——, and Coauthors, 2024b: TP-PROFILE: Monitoring the thermodynamic structure of the troposphere over the Third Pole. *Adv. Atmos. Sci.*, **41**, 1264–1277, https://doi.org/10.1007/s00376-023-3199-y.

Chen, Y., Y. Fu, T. Xian, and X. Pan, 2017: Characteristics of cloud cluster over the steep southern slopes of the Himalayas observed by CloudSat. *Int. J. Climatol.*, **37**, 4043–4052, https://doi.org/10.1002/joc.4992.

Chiaravalloti, F., L. Brocca, A. Procopio, C. Massari, and S. Gabriele, 2018: Assessment of GPM and SM2RAIN-ASCAT rainfall products over complex terrain in southern Italy. *Atmos. Res.*, **206**, 64–74, https://doi.org/10.1016/j.atmosres.2018.02.019.

Unauthenticated | Downloaded 04/10/25 01:22 AM UTC

Fang, J., W. Yang, Y. Luan, J. Du, and A. Lin, 2019: Evaluation of the TRMM 3B42 and GPM IMERG products for extreme precipitation analysis over China. *Atmos. Res.*, **223**, 24–38, https://doi.org/10.1016/j.atmosres.2019.03.001.

Fu, Y., and G. Liu, 2007: Possible misidentification of rain type by TRMM PR over Tibetan Plateau. *J. Appl. Meteor. Climatol.*, **46**, 667–672, https://doi.org/10.1175/JAM2484.1.

Guilloteau, C., E. Foufoula-Georgiou, P. Kirstetter, J. Tan, and G. J. Huffman, 2021: How well do multisatellite products capture the space–time dynamics of precipitation? Part I: Five products assessed via a wavenumber–frequency decomposition. *J. Hydrometeor.*, **22**, 2805–2823, https://doi.org/10.1175/JHM-D-21-0075.1.

——, ——, ——, ——, and ——, 2022: How well do multisatellite products capture the space–time dynamics of precipitation? Part II: Building an error model through spectral system identification. *J. Hydrometeor.*, **23**, 1383–1399, https://doi.org/10.1175/JHM-D-22-0041.1.

Huffman, G., and Coauthors, 2019: NASA Global Precipitation Measurement (GPM) Integrated Multi-Satellite Retrievals for GPM (IMERG). Algorithm Theoretical Basis Document (ATBD) version 06, NASA, 39 pp., https://pmm.nasa.gov/data-access/downloads/gpm.

Kazamias, A.-P., M. Sapountzis, and K. Lagouvardos, 2022: Evaluation of GPM-IMERG rainfall estimates at multiple temporal and spatial scales over Greece. *Atmos. Res.*, **269**, 106014, https://doi.org/10.1016/j.atmosres.2021.106014.

Kumar, M., Ø. Hodnebrog, A. S. Daloz, S. Sen, S. Badiger, and J. Krishnaswamy, 2021: Measuring precipitation in Eastern Himalaya: Ground validation of eleven satellite, model and gauge interpolated gridded products. *J. Hydrol.*, **599**, 126252, https://doi.org/10.1016/j.jhydrol.2021.126252.

Li, D., Y. Qi, and D. Chen, 2022: Changes in rain and snow over the Tibetan Plateau based on IMERG and ground-based observation. *J. Hydrol.*, **606**, 127400, https://doi.org/10.1016/j.jhydrol.2021.127400.

Li, L., X. Chen, Y. Ma, W. Zhao, H. Zuo, Y. Liu, D. Cao, and X. Xu, 2023: Implications for validation of IMERG satellite precipitation in a complex mountainous region. *Remote Sens.*, **15**, 4380, https://doi.org/10.3390/rs15184380.

Li, Y., W. Wang, H. Lu, S. Khem, K. Yang, and X. Huang, 2019: Evaluation of three satellite-based precipitation products over the lower Mekong River basin using rain gauge observations and hydrological modeling. *IEEE J. Sel. Top. Appl. Earth Obs. Remote Sens.*, **12**, 2357–2373, https://doi.org/10.1109/JSTARS.2019.2915840.

Liu, S., K. Hu, S. Zhang, and Y. Zeng, 2019: Comprehensive evaluation of satellite-based precipitation at sub-daily time scales over a high-profile watershed with complex terrain. *Earth Space Sci.*, **6**, 2347–2361, https://doi.org/10.1029/2019EA000855.

Meng, J., L. Li, Z. Hao, J. Wang, and Q. Shao, 2014: Suitability of TRMM satellite rainfall in driving a distributed hydrological model in the source region of Yellow River. *J. Hydrol.*, **509**, 320–332, https://doi.org/10.1016/j.jhydrol.2013.11.049.

O, S., and P.-E. Kirstetter, 2018: Evaluation of diurnal variation of GPM IMERG-derived summer precipitation over the contiguous US using MRMS data. *Quart. J. Roy. Meteor. Soc.*, **144**, 270–281, https://doi.org/10.1002/qj.3218.

Reichle, R. H., and R. D. Koster, 2004: Bias reduction in short records of satellite soil moisture. *Geophys. Res. Lett.*, **31**, https://doi.org/10.1029/2004GL020938.

Schamm, K., M. Ziese, A. Becker, P. Finger, A. Meyer-Christoffer, U. Schneider, M. Schröder, and P. Stender, 2014: Global gridded precipitation over land: A description of the new GPCC First Guess Daily product. *Earth Syst. Sci. Data*, **6**, 49–60, https://doi.org/10.5194/essd-6-49-2014.

Sunilkumar, K., A. Yatagai, and M. Masuda, 2019: Preliminary evaluation of GPM-IMERG rainfall estimates over three distinct climate zones with APHRODITE. *Earth Space Sci.*, **6**, 1321–1335, https://doi.org/10.1029/2018EA000503.

Tan, J., W. A. Petersen, and A. Tokay, 2016: A novel approach to identify sources of errors in IMERG for GPM ground validation. *J. Hydrometeor.*, **17**, 2477–2491, https://doi.org/10.1175/JHM-D-16-0079.1.

——, G. J. Huffman, D. T. Bolvin, E. J. Nelkin, and M. Rajagopal, 2021: SHARPEN: A scheme to restore the distribution of averaged precipitation fields. *J. Hydrometeor.*, **22**, 2105–2116, https://doi.org/10.1175/JHM-D-20-0225.1.

Xu, R., F. Tian, L. Yang, H. Hu, H. Lu, and A. Hou, 2017: Ground validation of GPM IMERG and TRMM 3B42V7 rainfall products over southern Tibetan Plateau based on a high-density rain gauge network. *J. Geophys. Res. Atmos.*, **122**, 910–924, https://doi.org/10.1002/2016JD025418.

Xu, X., X. Chen, D. Cao, Y. Liu, L. Li, and Y. Ma, 2023a: Comparisons of rainfall microphysical characteristics between the southeastern Tibetan Plateau and low-altitude areas. *J. Appl. Meteor. Climatol.*, **62**, 1591–1609, https://doi.org/10.1175/JAMC-D-23-0046.1.

——, ——, X. Zhao, D. Cao, Y. Liu, L. Li, and Y. Ma 2023b: Microphysical characteristics of snowfall on the southeastern Tibetan Plateau. *J. Geophys. Res. Atmos.*, **128**, e2023JD038760, https://doi.org/10.1029/2023JD038760.

Yang, Y., and D. Gao, 1996: A great geographical discovery in the end of 20th century—Demonstration on the Yarlung Zangbo river valley as the grandest canyon in the World. *Geogr. Res.*, **15** (4), 1–9.

Yatagai, A., K. Kamiguchi, O. Arakawa, A. Hamada, N. Yasutomi, and A. Kitoh, 2012: APHRODITE: Constructing a long-term daily gridded precipitation dataset for Asia based on a dense network of rain gauges. *Bull. Amer. Meteor. Soc.*, **93**, 1401–1415, https://doi.org/10.1175/BAMS-D-11-00122.1.

Zhang, C., X. Chen, H. Shao, S. Chen, T. Liu, C. Chen, Q. Ding, and H. Du, 2018: Evaluation and intercomparison of high-resolution satellite precipitation estimates—GPM, TRMM, and CMORPH in the Tianshan Mountain area. *Remote Sens.*, **10**, 1543, https://doi.org/10.3390/rs10101543.

Zhou, R., G. Wang, and S. Zhaxi, 2021: Cloud vertical structure measurements from a ground-based cloud radar over the southeastern Tibetan Plateau. *Atmos. Res.*, **258**, 105629.

Unauthenticated | Downloaded 04/10/25 01:22 AM UTC